Insights into the Control of Optoelectronic Properties in Mixed-stacking Charge-Transfer Complexes

Zongrui Wang,[a] Fei Yu,[a] Jian Xie,[a] Jianfeng Zhao,*[b] Ye Zou,[c] Zepeng Wang,[b] Qichun Zhang*[a]

In Memory of Professor Peiji Wu

Abstract: Although co-crystallization has provided a promising platform to develop new organic optoelectronic materials, it is still a big challenge to purposely design and achieve specific optoelectronic properties. In this contribution, we designed and synthesized a series of novel mixed-stacking cocrystals (TMFA, TMCA and TMTQ) and systematically investigated the regulatory effects of the acceptors on the co-assembled behaviors, charge transfer nature, energy level structures, and optoelectronic characteristics. Our results demonstrate that it is feasible to achieve effective charge-transport tuning and photo-response characteristics switching by carefully regulating the intermolecular charge transfer and energy orbitals. The inherent mechanisms underlying the change in these optoelectronic behaviors have been deeply analyzed and revealed, which would provide clear guidelines for future development of new optoelectronic materials. In addition, due to the excellent photo-responsive characteristic of TMCA, TMCA-based phototransistors have been deeply investigated upon the changes of light wavelength and optical powers, and TMCA displays the best performance among all reported cocrystals under UV illumination.

Introduction

Organic optoelectronic materials have been witnessed a significant growth in the past decades and have boosted the innovative and disruptive applications in the fields of OFETs (organic field-effect transistors),[1-3] OLEDs (organic light-emitting diodes),[4-5] OPVs (organic photovoltaics),[6-7] OPDs (organic photodetector)[8-9] and etc., owing to their superiorities in sensitive and selective light absorption and good photogeneration yield in a wide spectral region as well as their low-temperature, large-area and cost-effective processability for real industry. Although many successes in design and synthesis of new optoelectronic materials have been achieved, the traditional synthetic procedure is always grueling, time-consuming and resource-wasting. Considering these disadvantages, very recently, a distinctive but facile strategy of organic cocrystals (co-assembly of two or more components *via* noncovalent interactions) has been aroused.[10-11] This method has been well employed in the exploration of multifunctionalities such as electrical conductivity,[11-12] ambipolar charge transport,[13-14] light emision,[15-17] ferroelectricity,[18-20] photoconductivity[21] and etc., due to the induced versatile and unpredicted physicochemical properties from the synergistic and collective effects of every single component. Therefore, co-crystallization has become a proven emerging strategy to explore and investigate the new optoelectronic materials by rationally choosing appropriate starting materials and controlling their co-assembled structures. For example, through co-crystallization strategy, the switch of charge-transfer characteristics from p-type to ambipolar and n-type can be efficiently and economically fulfilled.[14, 22] However, although numerous encouraging results have been obtained in this field, it is still fumbling and elusive to clearly outline and predict this kind of switch. Thus, understanding what kind of situation and to what degree most likely lead to the conversion of charge-transport characteristics is highly deserved to be systematically investigated and addressed.

In addition to this, another intriguing point for the co-crystallization is that this system has offered a perfect platform to uncover the inherent mechanisms for the optoelectronic properties, due to the long-order and controllable molecular p-n junctions in cocrystals. Considering this, *Zhu*, *Hu* and co-workers have made some preliminary attempts, that is, in analogy with the bulk heterojunctions, the segregated donor (D) and acceptor (A) packing motif with the interdigitated network might benefit for the exciton separation as well as for photoconductivity and photovoltaic applications. On this basis, they synthesized the segregated-packing cocrystals of sulfur-bridged annulene DPTTA-C_{60}/C_{70} with light responsivity of 300 A/W and PCE of 0.27%.[13, 23] However, the photoconductivity nature is still unclear and they almost completely ignore in mixed-stacking co-crystals.[21, 24] Thus, it is highly deserved to input more efforts (including the more comprehensive insights into the structure-property relationship on the rationally co-assembled systems) to elucidate the underlying mechanisms of this specific optoelectronic property in cocrystals. Such mechanism is very important for future development of new optoelectronic materials with designed properties.

In this regard, we herein designed and synthesized a novel mixed-stacking system with the similar stoichiometric ratio (1:2 for D:A) of TMIQ-BQs, i.e., TMIQ-Chloranil (TMCA, CCDC number: 1953692), TMIQ-Fluoranil (TMFA, CCDC number: 1953693) and TMIQ-TCNQ (TMTQ, CCDC number: 1953694), by rationally

[a] Dr. Z. Wang, Dr. F. Yu, Dr. J. Xie, Prof. Q. Zhang
School of Materials Science and Engineering,
Nanyang Technological University, Singapore 639798, Singapore
E-mail: QCZHANG@ntu.edu.sg
[b] Prof. J. Zhao, Z. Wang
Key Laboratory of Flexible Electronics & Institute of Advanced Materials, Jiangsu National Synergetic Innovation Center for Advanced Materials, Nanjing Tech University, Nanjing 211816, P.R. China
E-mail: iamjfzhao@njtech.edu.cn
[c] Y. Zou
Beijing National Laboratory for Molecular Sciences, Key Laboratory of Organic Solids, Institute of Chemistry, Chinese Academy of Sciences, Beijing 100190, P.R. China

Supporting information for this article is given via a link at the end of the document

selecting a newly synthesized π-diindolodiazapentacene, 8,8,18,18-tetramethyl-8,18-dihydroindolo[1,2,3-fg]indolo[3',2',1':8,1]quinolino [2,3-b]acridine (TMIQ, Scheme S1) as the donor and three benzoquino-analogs (BQs) with different electron-withdrawing abilities as acceptors (*p*-chloranil, CA; *p*-fluoranil, FA; tetracyanoquinodimethane, TCNQ) (Figure 1). Their co-assembled behaviors, charge transfer nature, energy level structures, and optoelectronic characteristics are systematically investigated. We have fulfilled a regulatory of charge transport nature (from hole transport of TMCA and TMFA to electron transport of TMTQ) and photo-responsive characteristic (diminishing photo-response from TMCA and TMFA to TMTQ) through carefully controlling the intermolecular charge transfer (ICT) and molecular energy orbitals (MO). Moreover, we also revealed the "structure-property" relationship and gave a deeper understanding of the inherent mechanisms of charge-transport and optoelectronic characteristics switch in cocrystals with mixed-stacking modes. Finally, due to the excellent photo-response property of TMCA, the TMCA-based phototransistors are firstly fabricated and systematically studied and TMCA shows the best performance among all reported organic cocrystals.

Results and Discussion

Cocrystal Assembled Behavior: We firstly investigate the co-assembled behaviors of these cocrystals upon the different electron-withdrawing acceptors. As shown in Figure 1a, cocrystals of TMFA and TMCA (black rod-like crystals) were obtained at the same condition by mixing TMIQ (D) and Fluoranil or Chloranil (A) together with a molar ratio of 1:2 through a solution process method (Figure 1b, see details in Experimental Section of SI). Both X-ray photoelectron spectroscopy (XPS) analysis and Energy dispersive X-ray spectroscopy (EDS) element mapping (Figure S1, S2 and S3) proved the co-assembly of two components with the coexistence of elements N, O and F (or Cl) in the final product. Differential scanning calorimetry (DSC) measurement, with the smooth baseline and sharp melting peak (Figure S4), confirms the crystal structure without the included solvent molecules, and besides, the different melting point, comparing with those of single components, further denotes the significantly changed intermolecular interactions after co-crystallization,[25] indicating the formation of new lattice structure. Moreover, the typical powder X-ray diffraction (PXRD) profiles of cocrystals (TMFA and TMCA) exhibit different peaks from single components. These peaks are in line with the correspondingly simulated crystallographic data, further proving the success of co-crystallization process (Figure S5 and Figure S6).

Single crystal X-ray diffraction (SCXRD) is further performed to give insight of their molecular packing and driving forces for the co-assembled process. Both TMFA and TMCA co-crystallize into a $P2_1/c$ space group (monoclinic system) with the former unit-cell dimensions of a = 15.872(3) Å, b = 6.731(2) Å, c = 21.563(7) Å, α = 90°, β = 127.690(19)°, γ = 90°, and the latter cell parameters of a = 11.5873(16) Å, b = 6.8557(5) Å, c = 24.8500(19) Å, α = 90°, β = 90.062(6)°, γ = 90° (Table S1). Although the replacement of halogenated substitutes in acceptors (A) produces a similar co-assembled manner, molecular packing and interactions are significantly affected. Generally, in the crystal structure of TMCA, the D and A (with a 1:2 stoichiometry) stack alternately into columns along *b* axis with a mixed fashion, and the intermolecular

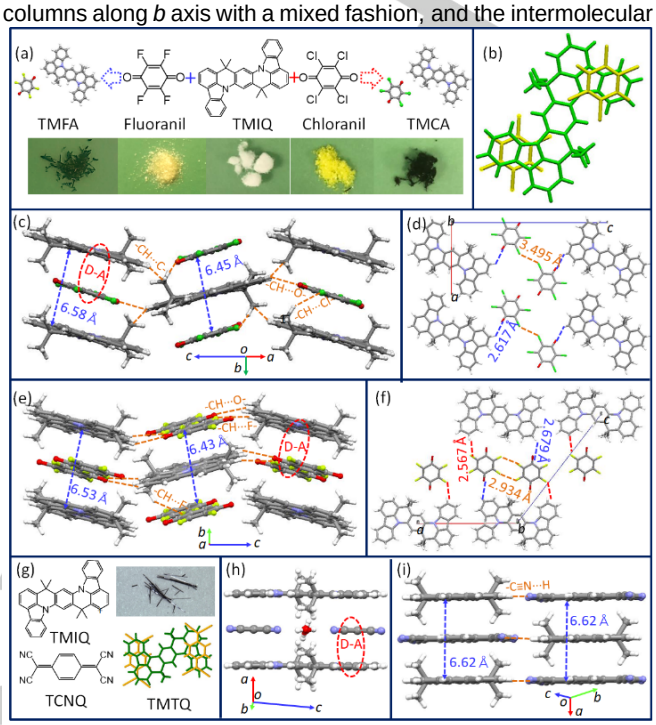

Figure 1. (a) The molecular structures of TMIQ, Chloranil, Fluoranil and (g) TCNQ as well as their cocrystal TMCA, TMFA and TMTQ, together with the optical graphs of their corresponding crystals. (b) Schematic diagram of the cocrystal with a stoichiometry 1:2 (D:A). Molecular packing in (c, d) cocrystal TMCA, (e, f) cocrystal TMFA and (h, i) cocrystal TMTQ.

D-A distance is around 3.22 (±0.07) Å, which is obviously smaller than the sum of the van der Waals radii of carbon atoms (3.4 Å),[26] indicating the strong D-A interactions (Figure 1c, Figure S7 and Figure S8). Besides, the neighboring columns communicate with each other *via* hydrogen -CH···O- (2.617 Å, TMIQ with CA), -CH···Cl- (2.872 Å and 2.926 Å, TMIQ with CA) and -CH···C- (2.875 Å, TMIQ with TMIQ) bonds (Figure 1d and Figure S8c). The synergy of these non-covalent interactions gives rise to the rod-like structures, which is also well proved from the morphology predictions conducted on the growth morphology algorithm of Material Studio software (Figure S11 and Table S1). In comparison, although TMFA also co-assembled into rod-like structure with D and A molecules packed along *b* axis in an alternate arrangement, TMIQ molecules rotate an nearly 90° angle with the long molecular side along *a* axis instead of along *c* axis in TMCA cocrystal, while the lateral acceptors still array along *a* axis, resulting in the more compact hydrogen-bond interactions for neighboring D-A molecules (-CH···O- of 2.679 Å, -CH···F- of 2.567 Å and 2.618 Å) but unfortunately losing the neighboring D-D communications (Figure 1e, f, Figure S9, S10, S11 and Table S2). Additionally, we also introduce a much stronger electron-withdrawing benzoquino-analog (TCNQ) as the acceptor to successfully harvest another black rod-like cocrystal TMTQ *via* a similar method with the identically stoichiometric ratio of 1:2 (Figure 1g). However, the change of TCNQ has induced the

interposition of H_2O in lattice, which brings about a perfect planar D with the deflection angle decreased to 0° (9.17 ° for TMCA and 7.68 ° for TMFA) and thereby leads to a very different space group of P-1 (triclinic system) for TMTQ with cell parameters of *a* = 6.6244(6) Å, *b* = 10.9794(10) Å, *c* = 16.4181(16) Å, *α* = 100.434(3)°, *β* = 95.274(4)°, *γ* = 106.759(3)°. The dominated driving force for the co-assembled behavior is D-A interaction with alternately arranged D and A molecules along *a* axis, while the neighboring columns communicate with each other through hydrogen -CN···H- bonds (D with A) (Figure 1h, Figure S12).

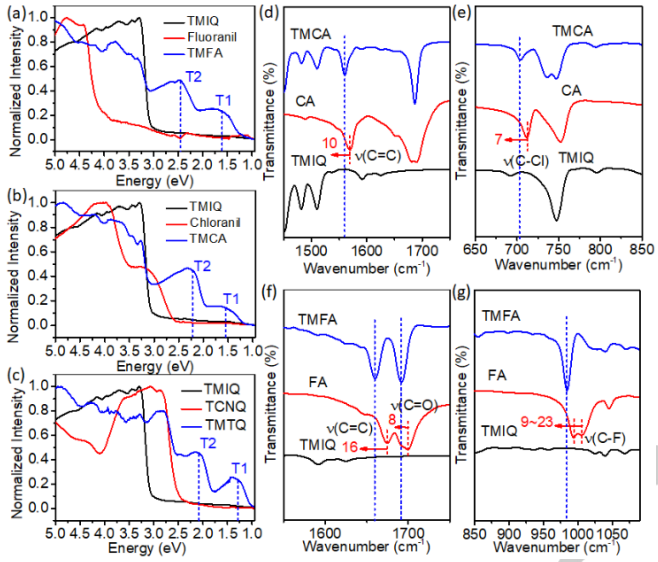

Figure 2. UV-vis-NIR absorption spectra of (a) TMCA; (b) TMFA and (c) TMTQ as well as their correspondingly constituted single components in solid state (samples in KBr to press pellets). Spatial enlarged FTIR spectra of powders for (d, e) TMIQ, Chloranil and the TMCA cocrystal, and (f, g) TMIQ, Fluroanil and TMFA cocrystal.

Intermolecular Charge Transfer and Molecular Energy Orbitals (MOs): The ICT behaviors upon different acceptors in the cocrystals are investigated due to their important role in determining the final optoelectronic properties.[15], [27-28] As depicted from UV-vis-NIR spectra analysis, although no significant CT behavior in TMFA was observed in a mixed solution (Figure S15a), the solid-state cocrystal exhibited a quite different scene, new absorptions of T1 and T2 appear at energies lower than the fundamental transitions of the isolated constituents (Figure 2a), signifying the typical CT characteristics. Similar phenomena were also observed in cocrystals of TMCA and TMTQ (Figure 2b, c and Figure S15). Notably, the optical band gap deduced from the onset of the initial absorption exhibits a reduced trend from TMFA (1.26 eV) to TMCA (1.20 eV) to TMTQ (1.05 eV), indicating a controllable CT interaction and energy band structures. Fourier transform infrared spectroscopy (FTIR) analysis further proved this charge transfer nature (Figure 2 and Figure S16, S17). For TMFA, there appeared apparent red-shifts in stretching vibrations of C=C ($\Delta\nu$=16 cm^{-1}), C=O ($\Delta\nu$=8 cm^{-1}) and C-F ($\Delta\nu$=9~23 cm^{-1}) of FA (suggesting the negatively charged co-former, Figure 2f and g),[29] as well as the significant blue-shifts of C-H, =C-H and N-H vibrations of TMIQ (indicating its positively charged, Figure S16).[30] These vibrational changes after co-crystallization attribute to CT transition through the DA, -CH···O- and -CH···F- interactions between D and A, which is well consistent with the analysis in the above-mentioned SCXRD.

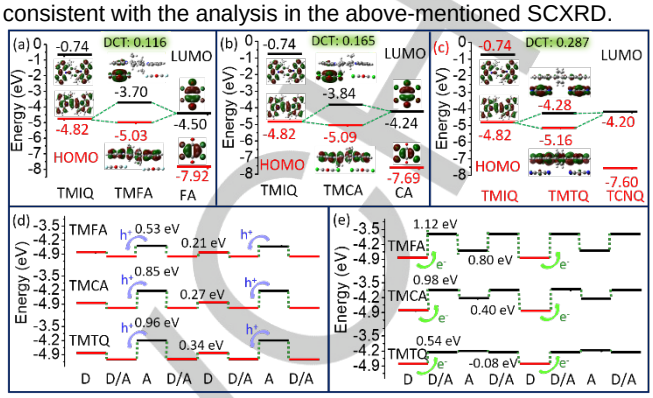

Figure 3. The molecular orbital energy level diagram of (a) TMFA, (b) TMCA and (c) TMTQ cocrystal and the correspondingly single components. The schematic diagram of simplified simulated energy orbital levels for the (d) hole charge transport and (e) electron charge transport along the mixed stacking direction for cocrystals TMFA, TMCA and TMTQ.

To more explicitly demonstrate this ICT transition and its effect on the molecular energy levels, the computational calculations are conducted at the Density Functional Theory (DFT) level with the hybrid B3LYP/6-31G** exchange-correlation functional on Gaussian 09 program and the corresponding scenario of single- and supramolecular hybrid orbitals is schematically illustrated in Figure 3. It states that the frontier MOs of D and A molecules are hybridized, leading to a substantial energy-level splitting. For example, TMFA cocrystal possesses the highest occupied molecular orbital (HOMO) of -5.03 eV (below that of TMIQ (-4.82 eV)), the lowest unoccupied molecular orbital (LUMO) of -3.70 eV (above that of FA component (-4.50 eV)), and a narrow band gap (in accordance with the occurrence of new sub-bandgap absorptions in UV/Vis/NIR spectroscopy, Figure 3a). This orbital hybridization is ascribed to the DA interaction, where the π-charge-transfer from TMIQ to FA induces the rearrangement of electron cloud and thus the formation of new orbitals.[31] Notably, in the cocrystal, the newly formed HOMO mainly distributes over the donor component, while LUMO mainly localizes on the acceptor, suggesting the weak CT interactions in the ground state.[32-33] Similar signatures are also found in orbital hybridization of TMCA and TMTQ cocrystals (Figure 3b and c), yet resulting in an decreased frontier hybrid orbitals and reduced band gaps (1.25 eV for TMCA and 0.88 eV for TMTQ), which can be attributed to the enhanced degree of charge transfer (DCT).[34] DCT upon different accepotors was also estimated by the Mulliken population analysis.[35] The calculated dipole moment (DM) exhibits an enlarged trend from 2.70 Debye for TMFA to 3.07 Debye for TMCA, then to 5.08 Debye for TMTQ (pointing to D, Figure S18), indicating a strengthened CT transition with the acceptors changed from FA to TCNQ. Correspondingly, the estimiated DCT increases from 0.116 for TMFA to 0.287 for TMTQ (0.165 for TMCA, Figure 3). In addition, accompanying with the inceased DCT and decreased frontier hybrid MOs, enlarged hole transport energy barriers (Figure 3d) but with more aligned electron transport MOs (Figure 3e) from cocrystal TMFA to TMCA

to TMTQ are observed, indicating the potential to switch the charge transport nature from hole transport to electron transport *via* preciously controlling the modified acceptors.

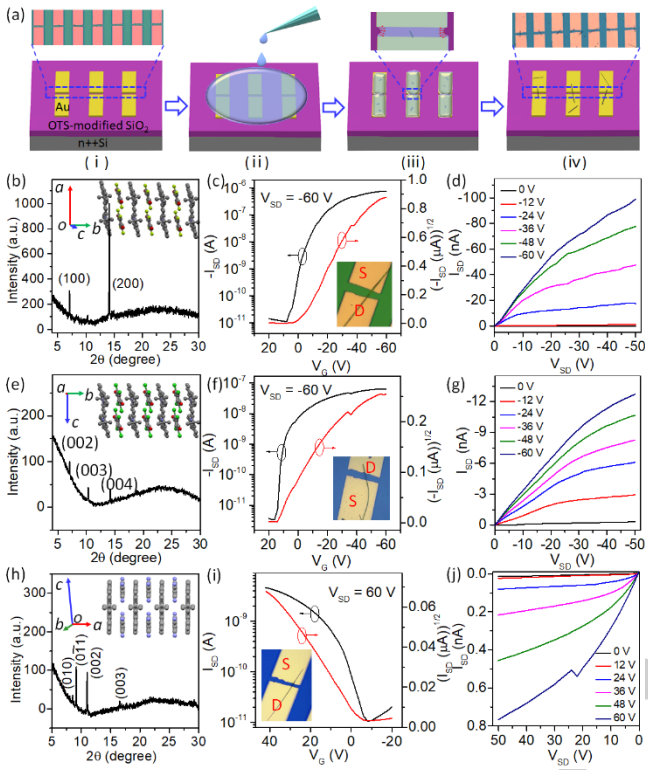

Figure 4. (a) Schematic diagram of the growth of cocrystal on the patterned electrodes by the confined self-assembly method. (i) The patterned source/drain electrodes on the OTS-modified SiO_2/Si substrates with the *W* of around 25 μm and *L* of about 5~7 μm. (ii) The dip-coating of cocrystal solution on the substrate. (iii) The growing micro/nanoribbons across the source/drain electrodes due to (iv) the formation of cocrystal arrays on the patterned source/drain electrodes (upper: physical map). XRD patterns of the self-assembled cocrystal micro/nano-rods on the OTS-modified SiO_2/Si substrates for (b) TMFA, (e) TMCA and (h) TMTQ. (c, f, i) Representative transfer and (d, g, j) output curves of the BC OFET based on (c, d) TMFA, (f, g) TMCA and (i, j) TMTQ micro-ribbons (insect: the corresponding device graph).

Charge Transport Characteristics: On account of above predictions, the inherent charge transport of the cocrystals are investigated on OFETs. Micro/nanocrystals suitable for the device fabrication are prepared through drop-casting the mixed solution onto the substrate, where TMIQ and co-formers recognize and self-assemble in an orderly way (long ribbon) *via* non-covalent interaction as behaved in bulk molecular co-crystals, which are different from the single-component crystals under the same condition (Figure S13 and S14). XRD patterns of these as-formed micro/nanocrystals demonstrate that D, A molecules are alternatively packed into micro-ribbons with the long edge (conduction direction) along the mixed-stack direction (*b* axis for TMFA, *b* axis for TMCA and *a* axis for TMTQ; Figure 3b, e and h), which provides a perfect platform to investigate the optoelectronic property regulatory. As well known, it has long been a big challenge to pattern and precisely register organic semiconductors within the transistor channel region over a large area, which is crucial in bottom-up based strategy.[36-37] Solvent wetting/dewetting surface treatment has been reported to be an efficient route to fulfill the precise positioning and patterning of crystals,[38-41] owing to the dewetting surface with poor affinity to organic solvents (while wetting surface with good affinity). On this basis, we herein explored a novel, facile and economic method to pattern bottom-contact (BC) OFETs with cocrystal arrays as depicted in Figure 4a, because the crystal is barely selectively nucleated and self-assembled on the wetting electrodes. Thus, this method can allow us to precisely register the crystalline domains across the channel regions when the satisfying conditions of *W* and *L* (see deails in SI) are met.

All measurements were conducted under ambient conditions. As predicted, the transfer and output curves (Figure 4c and d) for a typical device based on a TMFA micro-rod (Figure 4c inset) exhibit an ideally hole-transport characteristics in dark with the extracted saturated mobility up to 0.54 cm^2/Vs and an on/off ratio of above 10^5 (average of 26 devices: μ = 0.21 cm^2/Vs, Figure S18b). In comparison, the solely hole transport (Figure 4f, g) is also observed in TMCA-based device (Figure 4f inset) but with an inferior mobility (0.11 cm^2/Vs, the average of 20 devices: μ = 0.07 cm^2/Vs, Figure S20a) five-fold lower than that of TMFA. However, TMTQ micro-ribbon-based device exhibits an inverted polarity with the charge transport switched to electron transport (mobility up to 0.02 cm^2/Vs, Figure 4i). Meanwhile, the linear relation of I_{SD} with V_{SD} at the small bias for different gate voltages indicates a high-quality electrode/channel contact and an efficient charge injection (Figure 4d, g, j).[42] To illustrate this charge trasport characteristics of cocrystals, the alignment of the simplified energy orbital levels in the conduction (mixed-stacking) direction is displayed, where the charge transport adopts a hopping mechanism. As depicted in Figures 3d and e, the largest potential well (energy barrier) for holes (0.53 eV) is obviously much shallower (smaller) than that of electrons (1.12 eV) in TMFA, leading to its dominated hole tranport, and so does TMCA but with a larger energy barrier for holes (0.85 eV), accounting for its decreased hole transport. While for TMTQ, the energy barrier for electron transport (0.54 eV) is much smaller than that for hole tranport (0.96 eV), which results in the switch to electron transport behavior. The quantum simulations and first-principles electronic structure calculations are conducted based on DFT with the generalized gradient approximation (GGA) in the form of Perdew-Burke-Ernzerhof (PBE) function for exchange-correlation potential to more elaborately and intensively expore charge transport behavior. As depicted in Figures 5a, b and c, the largest dispersion contributing to the bandwidth is set along the alternate stacking direction (Figure S21), indicating that the electronic couplings for the carriers are mainly along this direction.[43] Here, we evaluated the effective electronic couplings (t^{eff}) for holes and electrons along the mixed-stacking direction through energy-splitting approach from the D-A-D and A-D-A clusters (Figures S22 and S23).[44] As seen in Figure S23, TMFA exhibits significantly better hole coupling (t^{eff}_{hole} of 11.16 meV) than that for electrons ($t^{eff}_{electron}$ of 5.31 meV), rationalizing the hole dominant transport in the experiment result. Meanwhile, for TMCA, the as-obtained much smaller t^{eff} for holes (7.76 meV) accounts very well for its inferior hole transport (Figure S22).

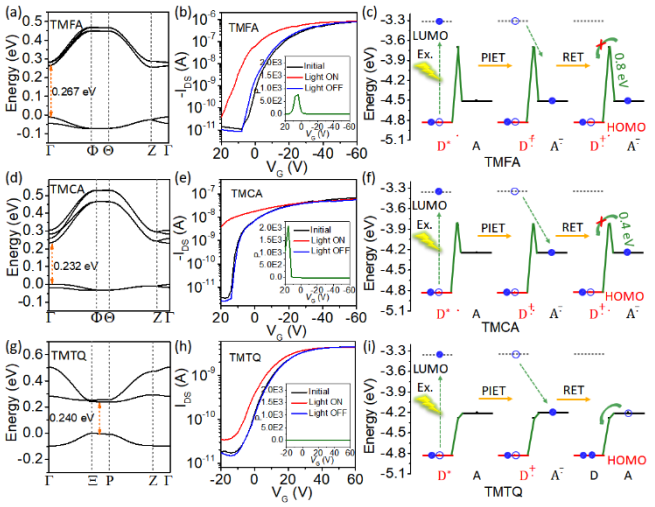

Figure 5. The band structures in (a) TMFA, (d) TMCA and (g) TMTQ system. The typical transfer curves of phototransistors based on (b) TMFA, (e) TMCA and (h) TMTQ microcrystals under dark and white light irradiation (0.23 mW/cm^2), inset is the accordingly photocurrent on/off ratio at different gate bias. The schematic diagram of simplified PIET process for (c) TMFA, (f) TMCA and (u) TMTQ including photoexcitation, excitons formation and recombination.

Optoelectronic Characteristics and Phototransistor Application: The photoresponsive behavior was further studied by exploring the photocurrent and the corresponding phototransistor schematic is depicted in Figure 6a. Under white light illumination, significantly enhanced photocarriers are generated in TMCA-based device with the photocurrent on/off ratio ($P = (I_{light} - I_{dark})/I_{dark}$) above 2×10^3 (V_G: 16 V, Figure 5e), which is among the highest values for all reported organic cocrystals,[1, 13, 16, 23-24] and the onset voltage (V_{on}) positively moves, indicating a photovoltaic effect.[4, 9] In comparison, TMFA-based device exhibits much inferior photoresponse with a decreased P (~500), while TMTQ shows disappeared photoresponse (Figure 5b, h), which is also evidenced from output curves (Figure S24). This clear distinction of optoelectronic property can be reflected on the photoinduced electron transfer (PIET)[45] process and the correspondingly simplified schematic representation is depicted in Figures 5c, f, and i. Typically, in our cases of cocrystals, upon photoexcitation of the donor to form the excited D*, there would be a charge redistribution between D* and A, which can occur a charge transfer from D* to ground-state A and result in the formation of a radical cation D^+ and a radical anion A^-. This process can enhance the charge carriers in solid state and therefore induce a photocurrent. Nevertheless, a reversed charge transfer (RCT) that causes the recombinantion of the electron-hole pair also happens at the same time, which is a critical factor to determine the eventual photoresponse. Apparently, in TMFA and TMCA, the energy barriers induced by the hybrid MOs at the D/A interface can hinder this RCT process, while in stark contrast, the loss of the barrier in TMTQ makes the recombination happen very easily, accounting for the disappeared photoresponsive property. Besides, it is worth noting that although TMFA owns a larger energy barrier (0.96 eV) than that of TMCA (0.4 eV), it exhibits an inferior photoresponse property, which can be atrributed to that the the network of D molecules, connected by the -CH···C- bonds, promotes the excitons seperation and offers additional transport paths for holes in TMCA (Figure S25).

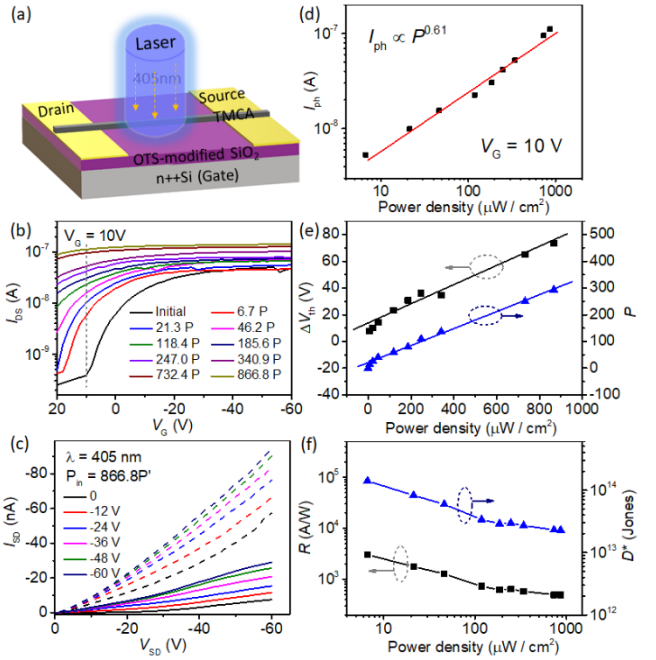

Figure 6. (a) Schematic diagram of TMCA microrod-based transistor under 405 nm laser illumination. (b) Transfer characteristics of phototransistors based on the cocrystal of TMCA under dark and different laser conditions (1P = 1 μW cm^{-2}). (c) Output curves of phototransistors under dark (solid line) and UV illumination (dashed) with the powder density of 866.8 μW/cm^2. (d) The photocurrent (I_{ph}) as a function of the light power density. (e) The threshold voltage shift (ΔV_{th}) and the photocurrent on/off ratio (P) versus different laser intensities. (f) The dependence of photoresponsivity (R) and specific detectivity (D^*) on different laser intensities.

The excellent photo-response of TMCA has supported opportunities to explore its application in phototransistors, and hence we systematically studied the TMCA-based phototransistors upon the change of light wavelength and optical powers (Figure 6). Under UV light illumination (405 nm) with the increasing power densities from 6.7 μW cm^{-2} to 866.8 μW cm^{-2}, the I_{light} is markedly enhanced and the according photocurrent ($I_{ph} = I_{light} - I_{dark}$) was instantly generated and gradually increased from 5.2 nA to 111 nA (V_G: 10 V, Figure 6b), and the maximum P (photocurrent on/off ratio) is estimated to be 353 (light intensity: 866.8 μW cm^{-2}, V_G: 20 V). I_{ph} can be expressed by a simple law ($I_{ph} \propto P^{0.61}$) from the plotted log-log scale of I_{ph} dependence on the light intensity and exhibits a sub-linear response, which can be ascribed to the process involved in the trap states induced by the defects or charge impurities present in the TMCA microrod and the semiconductor/dielectric interface (Figure 6d).[46-47] In addition, the threshold voltage shift (ΔV_{th}, towards more positive values) also exhibits an approximately linear relationship as a function of the power density and the maximum ΔV_{th} is up to 73 V (Figure 6e), which are derived from the trap sites filling effects by the photogenerated carriers that causes the injection and accumulation of additional holes in the active layer.[48] Besides, several other critical parameters to evaluate optoelectronic performance, i.e., photoresponsivity (R), external quantum

efficiency (EQE), detectivity (D^*) and linear dynamic range (LDR), are also performed.[49] R, an important factor to determine the efficacy of the generated I_{ph} upon the incident optical power and expressed as $R = I_{ph}/P_{in}$ (P_{in}, the incident optical power), displays a remarkable value of 3.0×10^3 A W^{-1} under the power density of 6.7 μW cm^{-2} at the depleted area (V_G = 10 V, V_{DS} = -60 V) (Figure 6f). Meanwhile, EQE, a measure of photoconductive gain, suggesting the generated number of the photo-induced charge carriers per incidence photon, is estimated to be about 2.4×10^6 % at power density of 6.7 μW cm^{-2} (V_G = -4 V, V_{DS} = -60 V) from the formula $EQE = (I_{ph}/e)/(P_{in}/hv) = hcR/e\lambda$, in which hc/λ is the photon energy of the excitation light and e is the electron charge (Figure S26). The large EQE is the result of the combined action of the charge traps in conduction channel and the band tail states near the band edge.[50-51] Under stronger excitation light, both R and EQE exhibit a decreased trend, which is due to the reduced lifetime caused by the enhanced recombination rate of the photocarriers.[51] LDR, described by the linear range ($I_{ph,max}$ to $I_{ph,min}$) of the photo-response *vs* the incident light irradiances (defined logarithmically according to $LDR = 20\lg(I_{ph,max}/I_{ph,min})$), is an important metric to describe the device light sensing characteristic (Figure 6d) and measured to be 27 dB. D^*, a very important figure of merit related to the sensitivity referring the distinguishment from the background noise, is given by $D^* = RA^{1/2}/(2eI_{dark})^{1/2}$ (A is the effective area of the device) when assuming the noise current mainly dominated by the shot noise from the dark current.[8] Figure 6f plots D^* of device as a function of different incident light intensities (V_G = 10 V), and it reaches maximal value of 1.4×10^{14} Jones under an incident light density of 6.7 μW cm^{-2}, obviously better than that for the commercial silicon device (≈10^{12} Jones).[47] It denotes that the cocrystals, possessing the mixed stacking modes with alternately strong DA overlap, still exhibit the appreciable photoconductivity. Moreover, the irradiation light of the phototransistors was found to be extended to the longer wavelength of 635 nm, under which it still exhibits the photosensitivity but the optoelectronic nature degenerated with maximum P of 105, R of 49 A W^{-1}, D^* of 2.04×10^{12} Jones and EQE of 9.5×10^3 % compared with those under 405 nm illumination (Figure S27 and Figure S28), illustrating the broadened wavelength absorption range. This result has important implications for the future optoelectronic materials synthesis.

Conclusions

In conclusion, we have designed and synthesized novel mixed-stacking cocrystals (TMCA, TMFA and TMTQ) based on TMIQ (D) and different co-formers (FA, CA and TCNQ). We tried to understand how co-formers with different electron-withdrawing abilities to affect the co-assembled behaviours, ICT nature, energy level structures, and optoelectronic characteristics. These crystals are co-assembled in a similar mode with the definite stoichiometric ratio (D:A = 1:2), which can give different charge transport nature (hole transport for TMFA and TMCA, and electron transport for TMTQ) and different photo-response characteristics (diminishing photo-response from TMCA and TMFA to TMTQ) through carefully regulating the intermolecular charge transfer and energy orbitals. Because these co-crystals possess the similar molecular packing in the conduction direction, they can provide us a perfect platform to elaborately reveal the inherent mechanisms underlying this switch of optoelectronic behaviours in a mixed-stacking motif. Such understanding is very important in the development of future optoelectronic materials. Finally, accounting for the excellent photo-response of TMCA, the TMCA-based phototransistors are deeply studied upon the changes of light wavelength and optical powers with the maximum P of 353, R of 3.0×10^3 A W^{-1}, D^* of 1.4×10^{14} Jones and EQE of 2.4×10^6 % under UV illumination. These values are the best ones among all results of the reported organic cocrystals. Our results prove that the co-crystallization can provide an alternative and valid approach to purposively control and develop new optoelectronic organic materials as well as explore the inherent physicochemical properties.

Acknowledgements

The authors first sincerely appreciate Prof. Mingtao Zhang (Nankai University), Caiqiao Dong (Nankai University) and Dr. Guankui Long's (Nanyang Technological University) help for calculation discussion. Q.Z. acknowledges financial support from AcRF Tier 1 (RG 111/17, RG 2/17, RG 114/16, RG 113/18) and Tier 2 (MOE 2017-T2-1-021 and MOE 2018-T2-1-070), Singapore. J. Zhao acknowledges financial support from Natural Science Foundation of Jiangsu Province (BK20171470).

Keywords: Co-crystallization, Charge transfer nature, Mixed-stacking mode, Charge transport switching, Phototransistor

[1] H. Dong, H. Zhu, Q. Meng, X. Gong, W. Hu, *Chem. Soc. Rev.* **2012**, *41*, 1754.
[2] D. Kufer, G. Konstantatos, *ACS Photonics* **2016**, *3*, 2197.
[3] H. Dong, X. Fu, J. Liu, Z. Wang, W. Hu, *Adv. Mater.* **2013**, *25*, 6158.
[4] K. J. Baeg, M. Binda, D. Natali, M. Caironi, Y. Y. Noh, *Adv. Mater.* **2013**, *25*, 4267.
[5] (a) X. Zhang, H. Dong, W. Hu, *Adv. Mater.* **2018**, *0*, 1801048; (b) J. Xiao, H. Yang, Z. Yin, J. Guo, F. Boey, H. Zhang, Q. Zhang, *J. Mater. Chem.* **2011**, *21*, 1423
[6] (a) O. Ostroverkhova, *Chem. Rev.* **2016**, *116*, 13279; (b) Y. Lin, Y. Li, X. Zhan, *Chem. Soc. Rev.* **2012**, *41*, 4245
[7] (a) H. Sun, X. Song, J. Xie, P. Sun, P. Gu, C. Liu, F. Chen, Q. Zhang, Z.-K. Chen, W. Huang, *ACS Appl. Mater. interfaces*, **2017**, *9*, 29924; (b) X. Fan, J. Gao, W. Wang, S. Xiao, C. Zhan, X. Lu, Q. Zhang, *Chem Asian J.*, **2019**, *14*, 1814.
[8] F. P. García de Arquer, A. Armin, P. Meredith, E. H. Sargent, *Nat. Rev. Mater.* **2017**, *2*, 16100.
[9] M. Buscema, J. O. Island, D. J. Groenendijk, S. I. Blanter, G. A. Steele, H. S. J. van der Zant, A. Castellanos-Gomez, *Chem. Soc. Rev.* **2015**, *44*, 3691.
[10] F. Wöhler, *Justus Liebigs Ann. Chem.* **1844**, *51*, 145.
[11] J. Ferraris, V. Walatka, Perlstei.Jh, D. O. Cowan, *J. Am. Chem. Soc.* **1973**, *95*, 948.
[12] L. B. Coleman, M. J. Cohen, D. J. Sandman, Yamagish.Fg, A. F. Garito, A. J. Heeger, *Solid State Commun.* **1973**, *12*, 1125.
[13] J. Zhang, J. H. Tan, Z. Y. Ma, W. Xu, G. Y. Zhao, H. Geng, C. A. Di, W. P. Hu, Z. G. Shuai, K. Singh, D. B. Zhu, *J. Am. Chem. Soc.* **2013**, *135*, 558.
[14] J. Zhang, J. Jin, H. Xu, Q. Zhang, W. Huang, *J. Mater. Chem. C* **2018**, *6*, 3485.
[15] W. Zhu, R. Zheng, Y. Zhen, Z. Yu, H. Dong, H. Fu, Q. Shi, W. Hu, *J. Am. Chem. Soc.* **2015**, *137*, 11038.

[16] L. Sun, W. Zhu, F. Yang, B. Li, X. Ren, X. Zhang, W. Hu, *Phys. Chem. Chem. Phys.* **2018**, *20*, 6009.
[17] H. Ye, G. Liu, S. Liu, D. Casanova, X. Ye, X. Tao, Q. Zhang, Q. Xiong, *Angew. Chem., Int. Ed.* **2018**, *57*, 1928.
[18] Y. Huang, Z. Wang, Z. Chen, Q. Zhang, *Angew. Chem., Int. Ed.* **2019**, *58*, 9696.
[19] S. Horiuchi, Y. Tokura, *Nat. Mater.* **2008**, *7*, 357.
[20] A. S. Tayi, A. Kaeser, M. Matsumoto, T. Aida, S. I. Stupp, *Nat. Chem.* **2015**, *7*, 281.
[21] V. M. Vincent, J. D. Wright, *J. Chem. Soc., Faraday Trans. 1* **1974**, *70*, 58.
[22] J. Zhang, P. Y. Gu, G. K. Long, R. Ganguly, Y. X. Li, N. Aratani, H. Yamada, Q. C. Zhang, *Chem. Sci.* **2016**, *7*, 3851.
[23] H. Zhang, L. Jiang, Y. Zhen, J. Zhang, G. Han, X. Zhang, X. Fu, Y. Yi, W. Xu, H. Dong, W. Chen, W. Hu, D. Zhu, *Adv. Electron. Mater.* **2016**, *2*, 1500423.
[24] Y. Wang, Y. Li, W. Zhu, J. Liu, X. Zhang, R. Li, Y. Zhen, H. Dong, W. Hu, *Nanoscale* **2016**, *8*, 14920.
[25] W. Zhu, L. Zhu, L. Sun, Y. Zhen, H. Dong, Z. Wei, W. Hu, *Angew. Chem., Int. Ed.* **2016**, *55*, 14023.
[26] W. Zhu, R. Zheng, X. Fu, H. Fu, Q. Shi, Y. Zhen, H. Dong, W. Hu, *Angew. Chem., Int. Ed.* **2015**, *54*, 6785.
[27] H. Jiang, P. Hu, J. Ye, K. K. Zhang, Y. Long, W. Hu, C. Kloc, *J. Mater. Chem. C* **2018**, *6*, 1884.
[28] M. S. Refat, O. B. Ibrahim, H. Al-Didamony, K. M. A. El-Nour, L. El-Zayat, *J. Saudi Chem. Soc.* **2012**, *16*, 227.
[29] A. Girlando, C. Pecile, *J. Chem. Soc., Faraday Trans. 2* **1975**, *71*, 689.
[30] Z. Wang, Y. Zou, W. Chen, Y. Huang, C. Yao, Q. Zhang, *Adv. Electron. Mater.* **2019**, *5*, 1800547.
[31] W. Zhu, L. Zhu, Y. Zou, Y. Wu, Y. Zhen, H. Dong, H. Fu, Z. Wei, Q. Shi, W. Hu, *Adv. Mater.* **2016**, *28*, 5954.
[32] H. Méndez, G. Heimel, S. Winkler, J. Frisch, A. Opitz, K. Sauer, B. Wegner, M. Oehzelt, C. Röthel, S. Duhm, D. Többens, N. Koch, I. Salzmann, *Nat. Commun.* **2015**, *6*, 8560.
[33] H. Mendez, G. Heimel, A. Opitz, K. Sauer, P. Barkowski, M. Oehzelt, J. Soeda, T. Okamoto, J. Takeya, J. B. Arlin, J. Y. Balandier, Y. Geerts, N. Koch, I. Salzmann, *Angew. Chem., Int. Ed.* **2013**, *52*, 7751.
[34] R. K. Behera, N. R. Goud, A. J. Matzger, J.-L. Brédas, V. Coropceanu, *J. Phys. Chem. C* **2017**, *121*, 23633.
[35] R. S. Mulliken, *The Journal of Chemical Physics* **1955**, *23*, 1833.
[36] S. Park, G. Giri, L. Shaw, G. Pitner, J. Ha, J. H. Koo, X. Gu, J. Park, T. H. Lee, J. H. Nam, Y. Hong, Z. Bao, *Proc. Natl. Acad. Sci.* **2015**, *112*, 5561.
[37] K. S. Park, J. Baek, Y. Park, L. Lee, J. Hyon, Y.-E. Koo Lee, N. K. Shrestha, Y. Kang, M. M. Sung, *Adv. Mater.* **2017**, *29*, 1603285.
[38] Y. Diao, B. C. K. Tee, G. Giri, J. Xu, D. H. Kim, H. A. Becerril, R. M. Stoltenberg, T. H. Lee, G. Xue, S. C. B. Mannsfeld, Z. Bao, *Nat. Mater.* **2013**, *12*, 665.
[39] A. L. Briseno, J. Aizenberg, Y.-J. Han, R. A. Penkala, H. Moon, A. J. Lovinger, C. Kloc, Z. Bao, *J. Am. Chem. Soc.* **2005**, *127*, 12164.
[40] Y. H. Kim, B. Yoo, J. E. Anthony, S. K. Park, *Adv. Mater.* **2012**, *24*, 497.
[41] O. Goto, S. Tomiya, Y. Murakami, A. Shinozaki, A. Toda, J. Kasahara, D. Hobara, *Adv. Mater.* **2012**, *24*, 1117.
[42] Z. Wang, H. Dong, Y. Zou, Q. Zhao, J. Tan, J. Liu, X. Lu, J. Xiao, Q. Zhang, W. Hu, *ACS Appl. Mater. Interfaces* **2016**, *8*, 7919.
[43] J. Zhang, H. Geng, T. S. Virk, Y. Zhao, J. H. Tan, C. A. Di, W. Xu, K. Singh, W. P. Hu, Z. G. Shuai, Y. Q. Liu, D. B. Zhu, *Adv. Mater.* **2012**, *24*, 2603.
[44] L. Zhu, Y. Yi, Y. Li, E.-G. Kim, V. Coropceanu, J.-L. Brédas, *J. Am. Chem. Soc.* **2012**, *134*, 2340.
[45] H. Lin, F. Bai, Eds., in *Electronic Process in Organic Solids*, Vol. Chapter 1, Wiely, VCH Verlag GmbH & Co. KGaA 2013.
[46] X. Zhou, L. Gan, W. Tian, Q. Zhang, S. Jin, H. Li, Y. Bando, D. Golberg, T. Zhai, *Adv. Mater.* **2015**, *27*, 8035.
[47] Q. Fu, C. Zhu, X. Zhao, X. Wang, A. Chaturvedi, C. Zhu, X. Wang, Q. Zeng, J. Zhou, F. Liu, B. K. Tay, H. Zhang, S. J. Pennycook, Z. Liu, *Adv. Mater.* **2018**, *31*, 1804945.
[48] C. Wang, X. Ren, C. Xu, B. Fu, R. Wang, X. Zhang, R. Li, H. Li, H. Dong, Y. Zhen, S. Lei, L. Jiang, W. Hu, *Adv. Mater.* **2018**, *30*, 1706260.
[49] F. Yang, S. Cheng, X. Zhang, X. Ren, R. Li, H. Dong, W. Hu, *Adv. Mater.* **2018**, *30*, 1702415.
[50] G. Konstantatos, M. Badioli, L. Gaudreau, J. Osmond, M. Bernechea, F. P. Garcia de Arquer, F. Gatti, F. H. Koppens, *Nat. Nanotechnol.* **2012**, *7*, 363.
[51] M. M. Furchi, D. K. Polyushkin, A. Pospischil, T. Mueller, *Nano Lett.* **2014**, *14*, 6165.

Entry for the Table of Contents

FULL PAPER

A novel series of mixed-stack cocrystals (TMFA, TMCA and TMTQ) are synthesized to systematically investigate the regulatory effects of the acceptors on the co-assembled behavior, energy level structures and thus on the optoelectronic characteristics with the hole/electron dominant transport switch and on/off of the photoresponse.

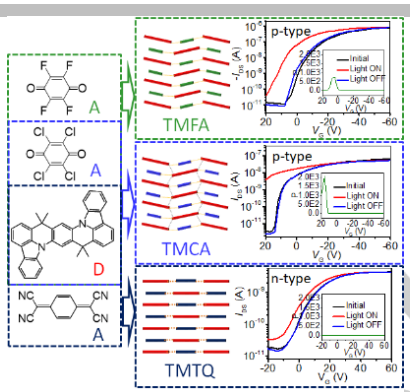

Zongrui Wang, Fei Yu, Jian Xie, Jianfeng Zhao, Ye Zou, Zepeng Wang, Qichun Zhang**

Page No. – Page No.

Insights into the Control of Optoelectronic Properties in Mixed-stacking Charge-Transfer Complexes